Chapter 6

Mass Spectrometric Detection of Oxidation Products and Intermediates of Aqueous Aerosol Iodide and/or Thiosulfate Reaction with Gaseous Ozone

Sections reprinted with permission from Enami, S.; Vecitis, C. D.; Cheng, J.; Hoffmann, M. R.; Colussi, A. J. *Journal of Physical Chemical A* **2007**, *111*, 50, 13032–13037.

Abstract

The intermediates ISO_3^- (m/z = 207) and $IS_2O_3^-$ (m/z = 239) generated in aqueous ($NaI/Na_2S_2O_3$) microdroplets traversing dilute O_3 gas plumes are detected via online electrospray mass spectrometry within ~ 1 ms, and their stabilities gauged by collisionally induced dissociation. The simultaneous detection of anionic reactants and the $S_2O_6^{2-}$, HSO_4^-, IO_3^-, and I_3^- products, as a function of experimental conditions, provides evidence for air-water interfacial reactions, as compared to strictly bulk aqueous reactions. For example, O_3(aq) reacts ~ 3 times faster with I^- than with $S_2O_3^{2-}$ in bulk solution; only $S_2O_3^{2-}$ is significantly depleted in the interfacial layers of $[I^-]/[S_2O_3^{2-}] = 10$ microdroplets below $[O_3(g)] \sim 50$ ppm. This suggests that either interfacial kinetics are at variance with bulk aqueous kinetics and/or I^- mediates that ozone oxidation of $S_2O_3^{2-}$.

Introduction

Atmospheric aerosols absorb and scatter solar radiation[1] and mediate important chemical processes[2,3,4,5]. For example, atmospheric SO_2 and NO_x can be oxidized in the gas-phase, but acid rain results from their faster processing in aqueous aerosol droplets[6,7,8.] However, the analysis of gas-aerosol reaction mechanisms and kinetics is assumed to follow concepts derived from studies performed in bulk aqueous solution[9,10]. However, the possibility of unique reaction mechanisms and enhanced chemical kinetics of air-water interfacial reactions, as well as the reduced water activity in atmospheric aerosol particles, should prevent the simple extrapolation of bulk data to the aerosol phase. The minimal examination of reactions specific to the air-water interface is a result of the technical difficulties associated with producing radially small aerosol particles under atmospherically relevant conditions in the laboratory and probing their chemical transformations while suspended in reactive atmospheres. Most studies, with a few exceptions[11,12,13], have monitored the uptake of reactive gases by stationary trains of ~10– 100 μm droplets[14] that would have exceedingly large settling velocities (~1 km day^{-1}), short residence times (i.e., negligible number densities in the atmosphere), and relatively low surface-area-to-volume ratios[15].

Here, we report experiments in which the chemical composition of aqueous droplets (r = 0.5 to 3.0 microns) undergoing chemical reaction with a reactive gas is directly monitored by electrospray mass spectrometry (ES-MS) in ~ 1–10 ms time frames. The fast oxidations of $I^-(aq)$ and $S_2O_3^{2-}(aq)$ by $O_3(g)$, which proceed at nearly diffusionally controlled rates in bulk solution[16], are studied by spraying droplets across O_3/air gas plumes. We detect and quantify anion reactants and products, as well as the previously

postulated short-lived reaction intermediates ISO_3^- and $IS_2O_3^-$. Our results show that this technique is capable of tracking chemical reactions in the condensed phase during fast aerosol-gas reactions. ES-MS has been previously used for online monitoring of thermal, electrochemical and photochemical reactions[17,18,19,20,21,22,23,24,25,26,27,28].

Experimental

The experimental setup is shown in Figures 6.1a and b. Aqueous solutions were pumped (50 μL min^{-1}) into the reaction chamber through a grounded stainless steel needle injector (~ 50 μM radius bore)[29]and pneumatically sprayed by means of coaxially flowing nebulizer gas. The difference between the exit velocities of the liquid jet (10.6 cm s^{-1}) and nebulizer gas (2.65×10^4 cm s^{-1}) is so large that the drag imposed on the liquid breaks it apart into micrometer size droplets. The terminal velocities of the microdroplets produced are ~ 10^2–10^3 cm s^{-1},[30] which lead to transit times around 1 to 10 ms across the ~ 0.5 cm wide ozone plume. The droplets are produced by fragmentation of electrically neutral solutions from a grounded injector, and are charged via statistical fluctuations that scale with (drop size)$^{-1/2}$ [31]. The ensemble of spray droplets is on average neutral, but individual droplets carry charges that follow a Gaussian distribution, as expected for a random process. For example, this phenomenon is the basis of the classical oil drop experiment performed by Millikan to determine the magnitude of the elementary charge[32] and leads to the charge of sea-sprayed aerosols. The finer sea water aerosol droplets, which will remain airborne the longest after generation during bubble bursting, are reported to be negatively charged[33]. It should be emphasized that charge separation during pneumatic nebulization of liquids does not produce highly charged droplets (10 to 100 charges per droplet vs. 10,000 charges per droplet) such as those created during

electrospray ionization using high-field nozzles[34]. The spray droplets eventually contract through solvent evaporation, a process regulated by ambient temperature and relative humidity, thereby increasing electrostatic repulsion among excess surface charges. In highly charged droplets, Coulomb explosions may occur, producing a distribution of smaller, charged droplets. Once charged droplets near radii on the nm scale, ion evaporation may occur, yielding hydrated, gas-phase ions[35]. Similar events will proceed in both sea-sprayed marine aerosols as they rise into the dry atmosphere, and our spray chamber as the droplets are electrostatically extracted into a high-temperature, high-flow-rate, dry-nitrogen gas stream. The drying events will generate smaller aerosols and eventually gas-phase ions whose chemical distribution is enriched in tensio- or surface active species. Thus, the ESMS technique effectively samples the interfacial layers of droplets.

Ozone was generated by flowing ultrapure O_2(g) (0.1 L/min, Air Liquide) through a commercial ozonizer (Ozone Solution), diluted tenfold with ultrapure N_2(g) (0.9 L/min) and quantified by UV absorption spectrophotometry (HP 8452) at 250 and 300 nm [absorption cross-sections σ(250 nm) = 1.1 x 10^{-17}, σ(300 nm) = 3.9 x 10^{-19} cm^2 $molecule^{-1}$ at 298 K][36] prior to entering the reaction chamber. In the text, the reported [O_3(g)] values, which correspond to the concentrations actually sensed by droplets in the reaction chamber, are estimated to be ~ 10 times smaller than the values determined from UV absorbances due to further dilution by the N_2 drying gas (Fig. 6.1a, 10 L/min). Gas flows were regulated by calibrated mass flow controllers (MKS). Typical instrumental parameters were as follows: drying gas temperature, 340 ^oC; Nebulizer pressure, 28 psi; collector capillary voltage, +3.5 kV; fragmentor voltage, 22 V. Solutions were prepared

with MilliQ water that had been previously purged with ultrapure N_2(g) for at least 30 min. NaI (> 99 %), Na_2SO_3 (> 98 %) and $Na_2S_2O_3$ (> 99.999 %) were obtained from Sigma-Aldrich. Solution pH was measured with a calibrated pH meter (VWR, SB21).

Results and Discussion

We have recently shown that I^- is rapidly oxidized to I_3^- and IO_3^- by O_3(g) at ppm levels in this experimental setup[37]. Thiosulfate is expected to react with O_3(g) at similar rates[38]. Since I_2/I_3^- also react rapidly with $S_2O_3^{2-}$, it should be possible to observe the transient intermediates $I_2S_2O_3^{2-}$ and $IS_2O_3^-$ proposed by Raschig a century ago to account for their slow conversion into tetrathionate (see also Table 6.1)[39,40,41,42,43].

$$I_2 + I^- \rightleftarrows I_3^- \qquad (6.1, 6.1')$$

$$I_2 + S_2O_3^{2-} \rightleftarrows I_2S_2O_3^{2-} \qquad (6.2, 6.2')$$

$$I_3^- + S_2O_3^{2-} \rightleftarrows I_2S_2O_3^{2-} + I^- \qquad (6.3, 6.3')$$

$$I_2S_2O_3^{2-} \rightleftarrows IS_2O_3^- + I^- \qquad (6.4, 6.4')$$

$$IS_2O_3^- + S_2O_3^{2-} \rightarrow I^- + S_4O_6^{2-} \qquad (6.5)$$

A similar mechanism has been proposed for the I_2/I_3^- + HSO_3^-/SO_3^{2-} reaction, which proceeds via the ISO_3^- intermediate[44,45,46,47]. The absorption spectra assigned by Packer and Anderson to the $I_2S_2O_3^{2-}$ and $IS_2O_3^-$ intermediates detected in their pulse radiolysis experiments[48], were found to be blue-shifted relative to those of I_3^- and I_2.

Identification of anion products and intermediates

Figure 6.2 shows the mass spectra of aqueous $Na_2S_2O_3$ microdroplets in the absence and presence of O_3(g). Signals at m/z = 112, 135, and 293, which are ascribed to $S_2O_3^{\cdot-}$, $NaS_2O_3^-$, and $Na_3(S_2O_3)_2^-$, respectively, are observed in the absence of O_3(g). We detect

the radical monoanion $S_2O_3^{\cdot-}$, rather than the closed-shell dianion $S_2O_3^{2-}$ (m/z = 56) in the ESMS of $Na_2S_2O_3$, in accord with previous reports[49,50]. Apparently, $S_2O_3^{2-}$(g) has negative electron affinity due to electrostatic repulsion between vicinal localized charges in $S{=}S(O)(O^-)_2$. The ready detection of $S_2O_8^{2-}$, in which charges are localized farther apart, supports this interpretation. Therefore, field ejection of $S_2O_3^{2-}$ from charged droplets[51] likely involves concerted electron transfer to the solvent, i.e.: $S_2O_3(H_2O)_n^{2-} \rightarrow S_2O_3^{\cdot-} + (H_2O)_n^-$. Thus, we consider $S_2O_3^{\cdot-}$ to be a valid marker of $S_2O_3^{2-}$ under present conditions. In the presence of O_3(g), new signals at m/z = 80, 97, 119, and 261 appear, which correspond to $S_2O_6^{2-}$, HSO_4^-, $NaSO_4^-$, and $Na_3(SO_4)_2^-$, respectively.

Figure 6.3 shows a mass spectrum of $NaI/Na_2S_2O_3$ microdroplets reacting with O_3(g). The m/z = 175 and 381 signals correspond to IO_3^- and I_3^-, while the signals at m/z = 207 and 239 are assigned to the I-S species ISO_3^- and $IS_2O_3^-$, respectively. The m/z = 207 signal, accompanied by m/z = 97, 175, and 381 signals, is also produced in the reaction of NaI/Na_2SO_3 microdroplets with O_3(g). All product signals disappear at once upon discontinuing O_3(g) injection.

The identity of S-containing species was confirmed from the relative intensities of their M and M+2 signals. Intensity ratios: M/M+2 = 100/4.4, 100/8.8, and 100/17.6 are expected for natural ^{34}S-abundance compounds containing one, two, and four S-atoms, respectively. The measured (112)/(114) = 100/9.9, (207)/(209) = 100/5.6, and (239)/(241) = 100/10.3 ratios are therefore consistent with species containing two, one, and two S-atom(s), respectively, and exclude $S_4O_6^{2-}$, $I_2S_2O_6^{2-}$ or $I_2S_4O_6^{2-}$ species. We infer that the m/z = 207 and 239 signals correspond to ISO_3^- and $IS_2O_3^-$, respectively.

Reaction Mechanism

Further information is gained by studying the dependence of signal intensities on $[O_3(g)]$. Reactant anion signal intensities at m/z = 112 ($S_2O_3^-$), 127 (I^-) and 135 ($NaS_2O_3^-$) decline with increasing $[O_3(g)]$, as shown in Figure 6.4a. Product and intermediate anion signal intensities at m/z = 80 ($S_2O_6^{2-}$), 97 (HSO_4^-), 119 ($NaSO_4^-$), 175 (IO_3^-), 381 (I_3^-), 207 (ISO_3^-), and 239 ($IS_2O_3^-$) are all enhanced upon increasing $[O_3(g)]$, as shown in Figure 6.4b and c. Note the upward inflections observed at ~ 50 ppm $O_3(g)$ in Figures 6.4b and c.

Figure 6.5 shows a plot of the $[HSO_4^-]/[S_2O_6^{2-}]$ ratio as function of $[O_3(g)]$. A nonvanishing value below ~ 50 ppm $O_3(g)$ is a direct indication that $S_2O_6^{2-}$ and HSO_4^- are primary species produced in competing pathways, eqs. 6.10a and b in Table 6.1[52]. The marked increase of this ratio at higher $[O_3(g)]$, however, shows that further HSO_4^- is produced in the oxidation of reactive byproducts. This interpretation is confirmed by the inertness of 0.1 mM $S_2O_6^{2-}$ toward O_3, together with the lack of HSO_4^- (m/z = 97) production below 420 ppm $O_3(g)$. Neither does a 0.25 mM $S_4O_6^{2-}$ solution, prepared by titration of 0.5 mM $S_2O_3^{2-}$ with I_3^-:[53]

$$I_3^- + 2S_2O_3^{2-} \rightarrow 3I^- + S_4O_6^{2-} \qquad (6.6)$$

and subsequently sprayed in the reaction chamber, react with $O_3(g)$. The m/z = 112 ($S_4O_6^{2-}$) and 97 (HSO_4^-) signal intensities remain constant below 520 ppm $O_3(g)$.

Figure 6.6 shows how ISO_3^-, $IS_2O_3^-$, HSO_4^-, and IO_3^- signal intensities vary with $[O_3(g)]$, and indicates that HSO_4^-, IO_3^-, ISO_3^-, and $IS_2O_3^-$ are later generation species whose rates of formation have a stronger, direct dependence on $[O_3(g)]$ than those of $S_2O_6^{2-}$ and I_3^-.

We recently found that in this setup the oxidation of I^- by $O_3(g)$ yields iodate, IO_3^-, and triiodide, I_3^- (R12-14)[29]. I_3^- is in equilibrium with I^- and I_2[54,55,56,57] (R1). I_3^- and/or I_2 can then react with HSO_3^- or $S_2O_3^{2-}$ according to reactions R2-R3 and R7-R8[28,32]. The fact that we do not observe $I_2SO_3^{2-}$ (m/z = 167) or $I_2S_2O_3^{2-}$ (m/z = 183) in NaI/Na_2SO_3 or NaI/$Na_2S_2O_3$ droplets in contact with $O_3(g)$ implies that their decomposition lifetimes are much shorter than ~ 1 to 10 ms under present conditions (eqs. 6.4' and 6.9); in accord with Margerum et al.[32] $I_2S_2O_3^{2-}$ is thermodynamically stable ($k_2/k_{-2} = K_2 = 3.2 \times 10^7$ M^{-1}), but kinetically reactive ($k_4/k_{-4} = K_4 = 0.245$ M). The dissociation equilibrium constant of $I_2S_2O_3^{2-}$, $K_4 = 0.245$ M, is ~ 100 times larger than that of I_3^-, $k_{-1}/k_1 = 1.39 \times 10^{-3}$ M.[58] Our results do not exclude, however, the participation of hypoiodous acid, HOI, which is considered to be more reactive than I_2 or I_3^- as oxidant.

$$HOI + S_2O_3^{2-} + H^+ \rightarrow IS_2O_3^- + H_2O \qquad (6.15)$$

The dependence of $IS_2O_3^-$ (m/z = 239) signal intensity in 30 μM $Na_2S_2O_3$ droplets as a function of [NaI] in the range of 1–300 μM, at constant [$O_3(g)$] = 300 ppm, is shown in Figure 6.7a. The observed exponential growth to a maximum is qualitatively consistent with the proposed mechanism of formation. Figure 6.7b shows the dependence of $IS_2O_3^-$ (m/z = 239) signal intensity in 30 μM NaI droplets as a function of [$Na_2S_2O_3$] in the range of 1–300 μM, at constant [$O_3(g)$] = 350 ppm. In contrast with the behavior observed in Figure 6.7a, $IS_2O_3^-$ peaks at [$Na_2S_2O_3$] ~ 100 μM. This response implies that $S_2O_3^{2-}$ participates both in the formation and destruction of $IS_2O_3^-$, and is consistent with the increasing role of eq. 6.5 at higher [$Na_2S_2O_3$][32]. From the reported value of $k_5 = 1.29 \times 10^6$ M^{-1} s^{-1}, we estimate that the half-life of $IS_2O_3^-$ in eq. 6.5 is ~ 5 ms at [$Na_2S_2O_3$] ~ 100 μM, which provides a direct measure of our temporal window. The rapid hydrolysis of

ISO_3^-, eq. 6.16, regenerates I^-,[44] and may be responsible for the results shown in Figure 6.8a.

Interfacial Reaction Kinetics

Figure 6.8 shows the dependence of $[I^-]$ and $[S_2O_3^{2-}]$ vs. $[O_3(g)]$ in three different solutions: $[NaI]_0 = [Na_2S_2O_3]_0 = 30$ μM (a), $[NaI]_0 = 10 \times [Na_2S_2O_3]_0 = 300$ μM (b), and $[Na_2S_2O_3]_0 = 10 \times [NaI]_0 = 300$ μM (c). $S_2O_3^{2-}$ undergoes significant oxidation in all cases over the entire $[O_3(g)]$ range covered in these experiments. In contrast, I^- oxidation begins above $[O_3(g)] \sim 50$ ppm in the a and b mixtures, and is fully inhibited in c. Since $O_3(aq)$ reacts ~ 3 times faster with I^- than with $S_2O_3^{2-}$ in the bulk (see Table 6.1) these observations imply that the interfacial layers of the droplets are predominantly populated by $S_2O_3^{2-}$ and/or that reactivities at the air-water interface are significantly different than in the bulk. Considering that the ratio of signal intensities, $I(S_2O_3^{\cdot-})/I(I^-) = 1.2 \pm 0.1$, in equimolar $Na_2S_2O_3$/NaI solutions is a direct measure of the relative affinities of $S_2O_3^{2-}$ and I^- for the interfacial layers of microdroplets, we must conclude that their relative reactivities toward $O_3(g)$ are indeed reversed relative to the bulk. Note that decrease of I^- at $[O_3(g)] \geq 50$ ppm in Figure 6.8a coincides with the onset of the $IS_2O_3^-$ and ISO_3^- in Figure 6.4c, supporting the proposed involvement of the products of I^- oxidation in their mechanism of formation.

Intermediate Stability

We probed the thermal stability of the ISO_3^-, $IS_2O_3^-$, and I_3^- in the gas-phase via collisional-induced dissociation experiments, in which the variation of ion signal intensities were recorded as function of fragmentor voltage (FV). FV is the electrical potential difference between the capillary exit and the first skimmer, a region where ions

are accelerated up to excess kinetic energies given by: $KE = FE \times q_i = ½\ m_i\ v_i^2$ (q_i is the charge, m_i the mass, and v_i the excess velocity of ion *i*, respectively). Molecular ions convert their excess KE into internal (vibrational/rotational) excitation during impact with (N_2) bath gas molecules prior to undergoing collisionally induced dissociation (CID)[59]. Figure 6.9a shows the dependence of m/z = 127 (I^-), 207 (ISO_3^-), 239 ($IS_2O_3^-$) and 381 (I_3^-) signal intensities on FV. The monotonous increase of the I^- signal reveals that ion collection efficiencies generally increase with FV. The maxima observed in the case of ISO_3^-, $IS_2O_3^-$, and I_3^- indicates, therefore, the onset of fragmentation. Curve deconvolution into two sigmoids, followed by the conversion of laboratory (KE) to center-of-mass (CEM) kinetic energies—CEM = m/(m + M) KE, where m = 28 is the molecular mass of the N_2 collider gas and M = 207, 239, or 381, the molecular masses of the various anions—leads to the fragmentation curves shown in Figure 6.9b. Threshold CEM energies are consistent with the reported values for $BDE(I^-–I_2)$ = 1.31 eV[60], and $BDE(I^-–SO_3)$ = 1.67 eV[61]. The fact that $IS_2O_3^-$ and ISO_3^- have similar stabilities in the gas-phase suggests the presence of weak I-S bonds in both species[32].

Figures

Figure 6.1. Diagram of electrospray and overall reactor setup. A) Schematic diagram of electrospraying chamber and O_3(g) injection system. B) An overview of the experimental setup. MFC stands for mass flow controller

A

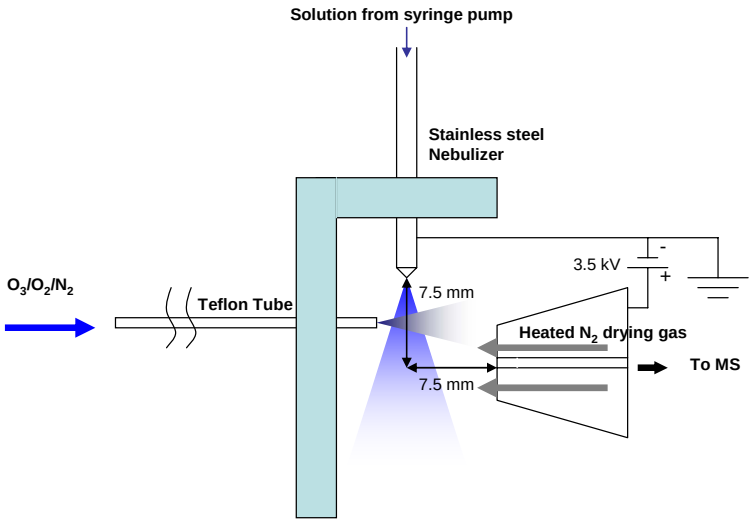

B

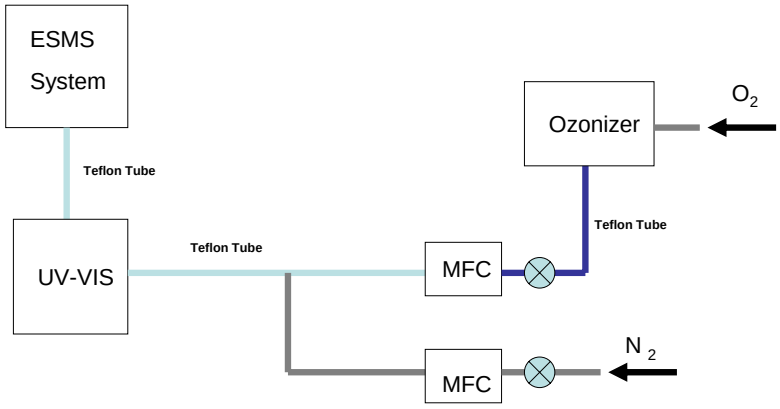

Figure 6.2. ESI-MS of aqueous $Na_2S_2O_3$ and gaseous O_3 reaction products. (100 μM $Na_2S_2O_3$, pH 6.2) droplets in the presence of 640 ppm O_3(g) (—), and in its absence (—). A) m/z = 112 ($S_2O_3^-$); B) 135 ($NaS_2O_3^-$); C) 293 [$Na_3(S_2O_3)_2^-$]; P) 80 ($S_2O_6^{2-}$); Q) 97 (HSO_4^-); R) 119 ($NaSO_4^-$); S) 261 [$Na_3(SO_4)_2^-$]

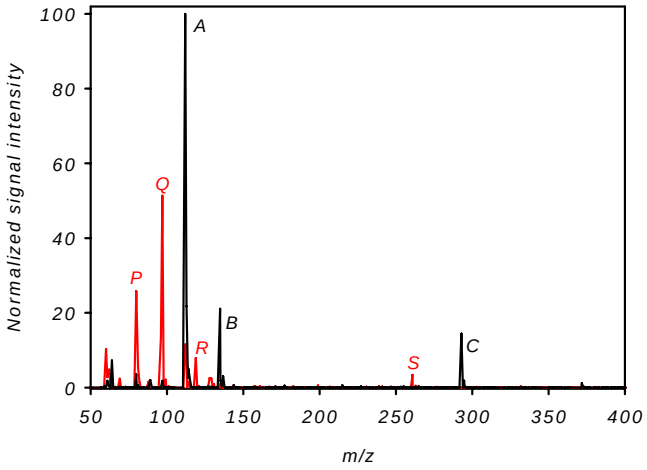

Figure 6.3. ESI-MS of aqueous $Na_2S_2O_3$-NaI droplets and gaseous O_3 reaction products. (100 μM $Na_2S_2O_3$ + 100 μM NaI, pH 6.2) microdroplets in the presence of 760 ppm O_3(g) (—), and in its absence (—). D) m/z = 127 (I^-); E) 277 (NaI_2^-); U) 159 (IO_2^-), V) 175 (IO_3^-); W) 381 (I_3^-); X) 207 (ISO_3^-); Y) 239 ($IS_2O_3^-$); Z) 255 ($IS_2O_4^-$)

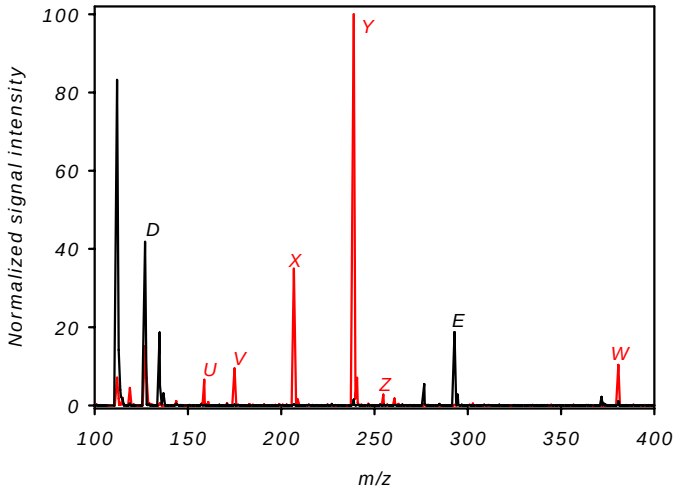

Figure 6.4. $Na_2S_2O_3$-$NaI_{(aq,drop)}$ and $O_{3(g)}$ reaction products vs. [$O_{3(g)}$]. (100 μM $Na_2S_2O_3$ + 100 μM NaI, pH 6.2) A) ESMS signal intensities at m/z = 112 ($S_2O_3^-$, ●), 127 (I^-, ○), and 135 ($NaS_2O_3^-$, ▲) vs. [O_3(g)]. B) ESMS signal intensities at m/z = 80 ($S_2O_6^{2-}$, Δ), 97 (HSO_4^-, ○), 175 (IO_3^-, ■), and 381 (I_3^-, □) vs. [O_3(g)]. C)ESMS signal intensities at m/z = 207 (ISO_3^-, ◊), 239 ($IS_2O_3^-$, ♦) vs. [O_3(g)]

A

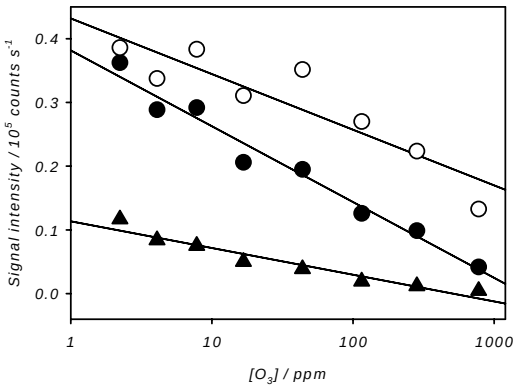

B

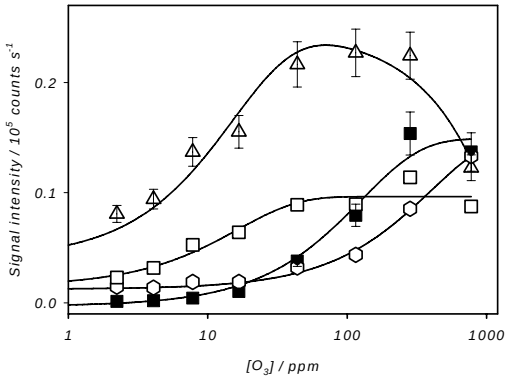

C

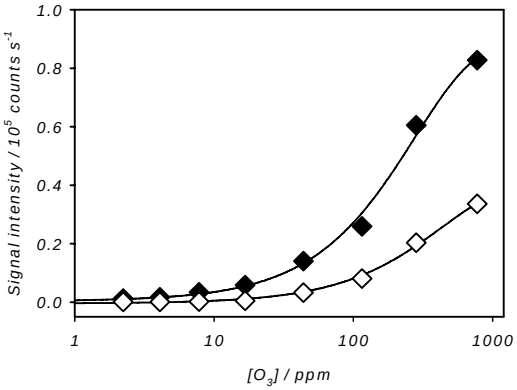

Figure 6.5. ESI-MS $HSO_4^-/S_2O_6^{2-}$ signal ratio vs. $[O_3(g)]$. Ratio of signal intensities at m/z = 97 and 80: $I(HSO_4^-)/I(S_2O_6^{2-})$ vs. $[O_3(g)]$ in (100 μM $Na_2S_2O_3$ + 100 μM NaI, pH 6.2) microdroplets

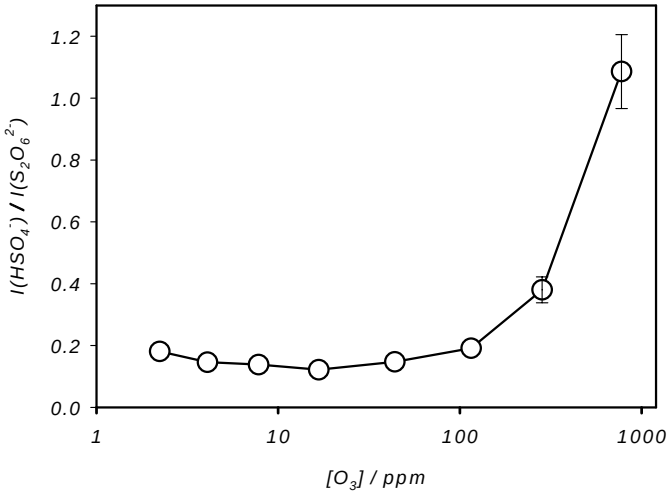

Figure 6.6. $Na_2S_2O_3$-$NaI_{(aq,drop)}$ and $O_{3(g)}$ reaction products vs. $[O_{3(g)}]$. Normalized ESI-MS signal intensities I at m/z = 97 (HSO_4^-), 175 (IO_3^-), 207 (ISO_3^-), and 239 ($IS_2O_3^-$) vs. $[O_3(g)]$ in (100 μM $Na_2S_2O_3$ + 100 μM NaI, pH 6.2) microdroplets

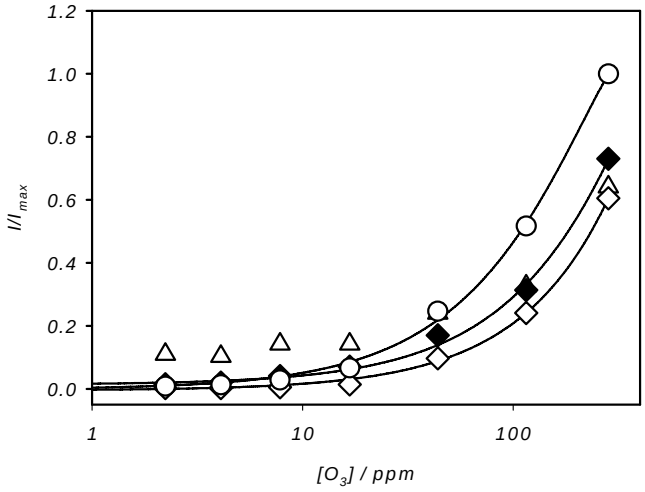

Figure 6.7. $IS_2O_3^-$ signal intensities vs. $[Na_2S_2O_3]$ and [NaI]. A) $[Na_2S_2O_3]_0$ in ($Na_2S_2O_3$ + 30 μM NaI, pH 6.2) microdroplets at $[O_3(g)]$ = 350 ppm, and B) $[NaI]_0$ in (30 μM $Na_2S_2O_3$ + NaI, pH 6.2) microdroplets at $[O_3(g)]$ = 300 ppm

A

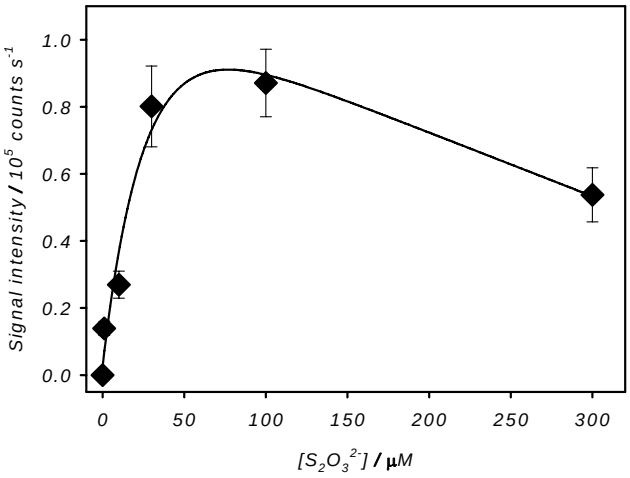

B

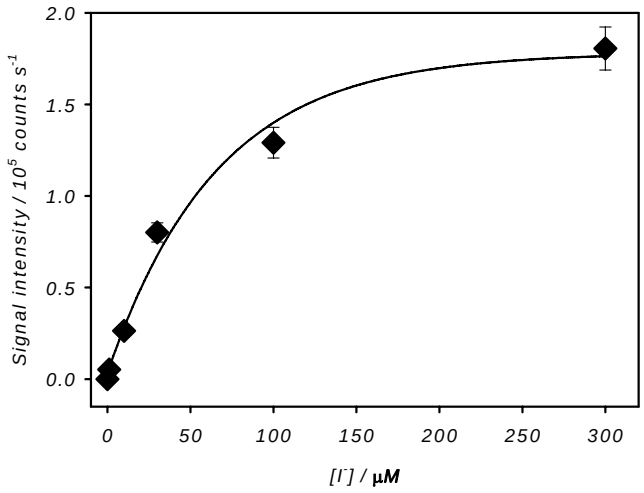

Figure 6.8. Normalized I^- and $S_2O_3^-$ ESI-MS signal intensities vs. $[O_{3(g)}]$. A) m/z = 127 (I^-) ($[NaI]_0 = [Na_2S_2O_3]_0$ = 30 μM) (Δ), ($[NaI]_0$ = 300, $[Na_2S_2O_3]_0$ = 30 μM) (○), and ($[NaI]_0$ = 30, $[Na_2S_2O_3]_0$ = 300 μM) (●), and B) m/z = 112 ($S_2O_3^-$) in: ($[NaI]_0 = [Na_2S_2O_3]_0$ = 30 μM) (▽), ($[NaI]_0$ = 300, $[Na_2S_2O_3]_0$ = 30 μM) (□), and ($[NaI]_0$ = 30, $[Na_2S_2O_3]_0$ = 300 μM) (■)

A

B

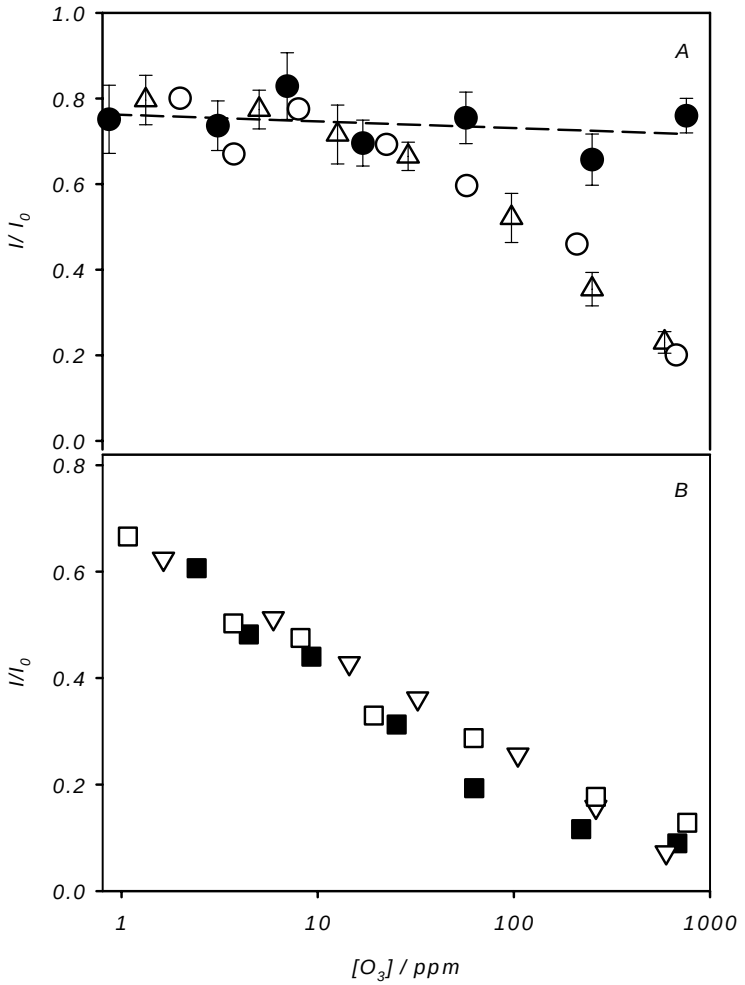

Figure 6.9. Collision-induced dissociation of $Na_2S_2O_3$-$NaI_{(aq)}$ and $O_{3(g)}$ products. A) ($[NaI]_0 = [Na_2S_2O_3]_0 = 100$ μM) microdroplets at $[O_3(g)] = 410$ ppm. I^- (○); ISO_3^- (▼); $IS_2O_3^-$ (▲); I_3^- (◊). B) ESI-MS signal intensities vs. center of mass energy. I_3^- (◊); ISO_3^- (▼); $IS_2O_3^-$ (▲)

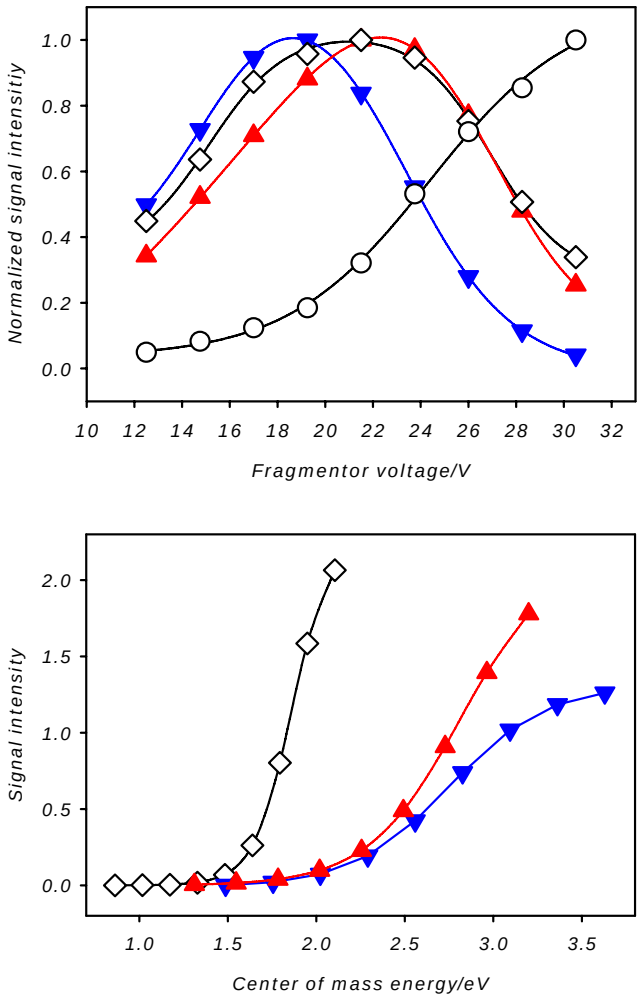

Tables

Table 6.1. Kinetic data for $Na_2S_2O_3$-$NaI_{(aq)}$ and $O_{3(g)}$ reactions at 298 K

eq#	Reaction	Rate or equilibrium constants (M, s units)	Ref.
6.1	$I_2 + I^- \rightleftarrows I_3^-$	721 M^{-1}	56
6.2 6.2’	$I_2 + S_2O_3^{2-} \rightleftarrows I_2S_2O_3^{2-}$	7.8×10^9 M^{-1} s^{-1} 2.5×10^2 s^{-1}	41
6.3 6.3’	$I_3^- + S_2O_3^{2-} \rightleftarrows I_2S_2O_3^{2-} + I^-$	4.2×10^8 M^{-1} s^{-1} 9.5×10^3 s^{-1}	41
6.4 6.4’	$I_2S_2O_3^{2-} \rightleftarrows IS_2O_3^- + I^-$	0.245 M	41
6.5	$IS_2O_3^- + S_2O_3^{2-} \rightarrow I^- + S_4O_6^{2-}$	1.3×10^6 M^{-1} s^{-1}	41
6.6	$I_3^- + 2S_2O_3^{2-} \rightarrow 3I^- + S_4O_6^{2-}$	N/A	41
6.7	$I_2 + HSO_3^- \rightarrow I_2SO_3^{2-} + H^+$	1.7×10^9 M^{-1} s^{-1}	
6.8	$I_3^- + HSO_3^- \rightarrow I^- + I_2SO_3^{2-} + H^+$	1.5×10^7 M^{-1} s^{-1}	44
6.9	$I_2SO_3^{2-} \rightarrow ISO_3^- + I^-$	N/A	44
6.10a 6.10b	$S_2O_3^{2-} + O_3 \rightarrow S_2O_6^{2-}$ $\rightarrow SO_4^{2-} + SO_2$	3.7×10^8 M^{-1} s^{-1}	38
6.11	$SO_2 + H_2O \rightleftarrows HSO_3^- + H^+$	1.3 x 10^{-2} M	62
6.12	$I^- + O_3 + H^+ \rightarrow HOI + O_2$	1.2×10^9 M^{-1} s^{-1}	16
6.13	$HOI + 2O_3 \rightarrow IO_3^- + 2O_2 + H^+$	3.6×10^4 M^{-1} s^{-1}	63
6.14	$HOI + I^- + H^+ \rightarrow I_2 + H_2O$	4.4×10^{12} M^{-2} s^{-1}	64
6.15	$HOI + S_2O_3^{2-} + H^+ \rightarrow IS_2O_3^- + H_2O$	N/A	
6.16	$ISO_3^- + H_2O \rightarrow I^- + SO_4^{2-} + 2H^+$	298 s^{-1}	44

References

(1) Satheesh, S. K.; Moorthy, K. K. *Atmos. Environ*. **2005**, *39*, 2089.

(2) Herrmann, H.; *Chem. Rev.* **2003**, *103*, 4691.

(3) Reid, J. P.; Sayer, R. M. *Chem. Soc. Rev*. **2003**, *32*, 70.

(4) Nissenson, P.; Knox, C. J. H.; Finlayson-Pitts, B. J.; Phillips, L. F.; Dabdub, D. *Phys. Chem Chem. Phys.* **2006**, *8*, 4700.

(5) Pilinis, C.; Pandis, S. N.; Seinfeld, J. H. *J. Geophys. Res.* **1995**, *100*, 18739.

(6) Hoffmann, M. R.; Edwards, J. *J. Phys. Chem.* **1975**, *79*,2096.

(7) Mcardle, J. V.; Hoffmann, M. R. *J. Phys. Chem*. **1983**, *87*, 5425.

(8) Hoffmann, M. R. *Atmos. Environ*. **1986**, *20*, 1145.

(9) Hunt, S. W.; Roeselova, M.; Wang, W.; Wingen, L. M.; Knipping, E. M.; Tobias, D. J.; Dabdub, D.; Finlayson-Pitts, B. J. *J. Phys. Chem. A,* **2004***, 102,* 11559.

(10) Hu, J. H.; Shi, Q.; Davidovitz, P.; Worsnop, D. R.; Zahniser, M. S.; Kolb, C. E., *J. Phys.Chem.* **1995**, *99*, 8768.

(11) Schütze, M.; Herrmann, H. *Phys. Chem. Chem. Phys.* **2006**, *4*, 60.

(12) Tolocka, M. P.; Saul, T. D.; Johnston, M. V. *J. Phys. Chem. A* **2004**, *108*, 2659.

(13) González-Labrada, E.; Schmidt, R.; DeWolf, E. *Chem.Comm*. **2006**, *23,* 2471.

(14) Davidovits, P.; Kolb, C. E.; Williams, L. R.: Jayne, J. T.; Worsnop, D. R. *Chem. Rev*. **2006**, *106*, 1323.

(15) Finlayson-Pitts, B. J.; Pitts, J.N. *Chemistry of the upper and lower atmosphere,* Academic Press: San Diego, California, **2000**; p. 364.

(16) Liu, Q.; Schurter, L. M.; Muller, C. E.; Aloisio, S.; Francisco, J. D.; Margerum, D.W. *Inorg. Chem.* **2001**, *40*, 4436.

(17) Espenson, H. E.; Tan, H.; Mollah, S.; Houk, R. S.; Eager, M. D. *Inorg. Chem.* **1998**, *37*, 4621.

(18) Bakhtiar, R.; Hop, C. E. C. A. *J. Phys. Org. Chem*. **1999**, *12*, 511.

(19) Arakawa R.; Liu, J.; Mizuno, K.; Inoue, H.; Doe H.; Matsuo, T. *Int. J. Mass Spectrom*. **1997**, *160*, 371. **B.** Arakawa, R.; Tachiyashiki, S.; Matsuo, T. *Anal. Chem*. **1995**, *67*, 4133. **C.** Arakawa, R.; Mimura, S.; Mastsubayashi, G.; Matsuo, T. *Inorg. Chem*. **1996**, *35*, 5725. **D.** Arakawa, R.; Matsuda, F.; Mastsubayashi, G. *Am. Soc. Mass Spectrom*. **1997**, *8*, 713 .

(20) Aliprantis, A. O.; Canary, J. W. *J. Am. Chem. Soc*. **1994**, *116*, 6985.

(21) Brum, J.; Dell'Orco, P.; Lapka, S.; Muske, K.; Sisko, J. *Rapid Commun. Mass Spectrom*. **2001**, *15*, 1548.

(22) Zechel, D. L.; Konermann, L.; Withers, S. G.; Douglas, D. J. *Biochemistry* **1998**, *37*, 7664.

(23) Xu, X.; Lu, W.; Cole, R. B. *Anal. Chem*. **1996**, *68*, 4244.

(24) Brum, J.; Dell'Orco, P. *Rapid Commun. Mass Spectrom*. **1998**, *12*, 741.

(25) Volmer, D. A. *J. Chromatogr. A* **1998**, *794*, 129.

(26) Santos, L. S.; Knaack, L.; Metzger, J. O. *Int. J. Mass. Spec.* **2005**, *246*, 84.

(27) Ding, W.; Johnson, K. A.; Kutal, C.; Amster, I. J. *Anal. Chem.* **2003,** *75*, 4624.

(28) Thomas, M. C.; Mitchell, T. W.; Blanksby, S. J. *J. Am. Chem. Soc*. **2005,** *128*, 58.

(29) Cheng. J.; Vecitis, C. D.; Hoffmann, M. R.; Colussi, A. J. *J. Phys. Chem. B.* **2006**, *110*, 25598.

(30) Kahen, K.; Jorabchi, K.; Gray, C.; Montaser, A. *Anal. Chem.* **2004**, *76*, 7194.

(31) Dodd, E. E. *J. Appl. Phys.* **1953**, *24*, 73.

(32) Millikan, R. A. *Science* **1910**, *32*, 436.

(33) Reiter, R. *J. Geophys. Res.* **1994**, *99*, 10807.

(34) Fenn, J. B. *J. Am. Soc. Mass Spectrom.* **1993**, *4*, 524.

(35) Kebarle, P. *J. Mass Spectrom.* **2000**, *35*, 804.

(36) Sander, S. P., et al. *Chemical Kinetics and Photochemical Data for Use in Stratospheric Modeling, Evaluation 15*; Jet Propulsion Laboratory: Pasadena, CA, **2006**.

(37) Enami, S.; Vecitis, C. D.; Cheng. J.; Hoffmann, M. R.; Colussi, A. J. *J. Phys. Chem. A,* **2007**, *111*, 50, 13032.

(38) Muller, B.; Heal, M. R., *Phys. Chem. Chem. Phys.* **2002**, *4*, 3365.

(39) Raschig, F. *Chem. Ztg.* **1908**, *32*, 1203.

(40) Raschig, F. *Ber. Dtsch. Chem. Ges.* **1915**, *48*, 2088.

(41) Scheper, W. M.; Margerum, D. W. *Inorg. Chem*. **1992**, *31*, 5466.

(42) Dodd, G.; Griffith, R. O. *Trans. Faraday. Soc.* **1949**, *45*, 546.

(43) Awtrey, A.; Connick, R. E. *J. Am. Chem. Soc*. **1951**, *73*, 1341.

(44) Yiin B. S.; Margerum, D. W. *Inorg. Chem.* **1990**, *29*, 1559.

(45) Landolt, H. *Ber. Dtsch. Chem. Ges.* **1886**, *19*, 1317.

(46) Bunau, G.V.; Eigen, M. *Z. Physik. Chem. (Frankfurt)* **1962**, *32*, 27.

(47) Inoue, H.; Sudo, Y. *Kogyo Kagaku Zasshi* **1967,** *70*, 123.

(48) Packer, J. E.; Anderson, R. F. *Aust. J. Chem*. **1997,** *50*, 435.

(49) Stewart, I. I.; Barnett, D. A.; Horlick, G. *J. Anal. Atom. Spec.* **1996**, *11*, 877.

(50) Agnes, G. R.; Stewart, I. I.; Horlick, G. *Appl. Spec.* **1994**, *48*, 1347.

(51) Kebarle, P. *J. Mass Spectrom.* **2000**, *35*, 804.

(52) *Gmelins Handbuch der anorganischen Chemie*, *Schwefel*, Teil B, Lieferung 2;

Verlag: Weinheim; 1960, p. 896, and references therein.

(53) Harris, W. E.; Daniel, C. Q*uantitative Chemical Analysis,* 3rd ed.; Freeman: New York, **1991**.

(54) Myers, O. E. *J. Chem. Phys*. **1958**, *28*, 1027.

(55) Ramette, R. W.; Sandford, Jr., R. W. **1965**, *87*, 5001.

(56) McIndoe, J. S.; Tuck, D. G. *Dalton Trans*. **2003**, *2*, 244.

(57) Troy, R. C.; Kelly, M. D.; Nagy, J. C.; Margerum, D. W. *Inorg. Chem.* **1991,** *30,* 4838.

(58) Ramette, R. W.; Sandford, R. W. *J. Am. Chem. Soc*. **1965**, *87*, 5001.

(59) Schneider B. B.; Chen. D. Y. *Anal. Chem*. **2000**, *72*, 791.

(60) Nizzi, K. E., Pommerening, C. A., Sunderlin, L. S., *J. Phys. Chem. A*, **1998**, *102*, 7674.

(61) Hao, C., Gilbert, T. M., Sunderlin, L. S., *Can. J. Chem.* **2005**, *83*, 2013

(62) Sillén, G. H.; Martell, A. E. *Stability Constants of Metal-Ion Complexes*, Special Publication 17; Chemical Society: London, **1964**.

(63) Bichsel, Y.; von Gunten, U.; *Environ. Sci. Technol*. **1999**, *33*, 4040.

(64) Eigen, M.; Kustin, K. *J. Am. Chem. Soc.* **1962**, *84*, 1355.